

1 **Age and Sex-Dependent Differences in Human Cardiac Matrix-Bound Exosomes Modulate Fibrosis**
2 **through Synergistic miRNA Effects**

3

4 Authors: George Ronan^{1,2}, Gokhan Bahcecioglu^{2,3}, Jun Yang⁴, Pinar Zorlutuna^{1,2,3,4*}

5 ¹Bioengineering Graduate Program, University of Notre Dame, Notre Dame, IN, 46556, USA

6 ²Department of Aerospace and Mechanical Engineering, University of Notre Dame, Notre Dame, IN,
7 46556, USA

8 ³Harper Cancer Research Institute, University of Notre Dame, Notre Dame, 46556, USA

9 ⁴Department of Chemical and Biomolecular Engineering, University of Notre Dame, Notre Dame, IN,
10 46556, USA

11 *Corresponding Author: Pinar Zorlutuna

12

13 George Ronan (ORCID: 0000-0003-1485-0914): gronan@nd.edu

14 Gokhan Bahcecioglu (ORCID: 0000-0002-6228-4745): gbahceci@nd.edu

15 Jun Yang: jyang26@nd.edu

16 Pinar Zorlutuna (ORCID: 0000-0002-3122-7553): pzorlutuna@nd.edu

17

18 Data Availability Statement: All data required for production of the manuscript is included in this
19 submission. Additional raw data can be provided upon request.

- 20 Funding Statement: Research reported in this publication was supported by NSF-CAREER Award #
21 1651385, NSF CBET Award # 1805157 and NIH Award # 1 R01 HL141909-01A1
- 22 Competing Interests Statement: The authors have no competing interest to disclose.
- 23 Ethics Statement: All animal work was performed under the approved IACUC protocol number 18-05-4687
- 24
- 25 Keywords: Aging, Exosomes, ECM, Cardiac, Fibrosis

26 **ABSTRACT**

27 Aging is a risk factor for cardiovascular disease, the leading cause of death worldwide. Cardiac fibrosis is
28 a harmful result of repeated myocardial infarction that increases risk of morbidity and future injury.
29 Interestingly, rates of cardiac fibrosis are different between young and aged individuals, as well as men
30 and women. Here, for the first time, we identify and isolate matrix-bound extracellular vesicles from the
31 left ventricles (LVs) of young or aged men and women. These LV vesicles (LVVs) show differences in
32 morphology and content between these four cohorts. LVVs effects on fibrosis were also investigated *in*
33 *vitro*, and it was shown that aged male LVVs were pro-fibrotic, while other LVVs were anti-fibrotic. miRNAs
34 identified from these LVVs could partially recapitulate these effects together, but not individually, and
35 confer other benefits. These data suggest that synergistic effects of matrix-resident exosomal miRNAs
36 may influence the differential clinical response to MI.

37 **INTRODUCTION**

38 Cardiovascular disease is the leading cause of death in the United States and worldwide, with myocardial
39 infarction (MI) as the chief cause of death among CVDs¹. While initial incidence of MI tends to be non-
40 fatal, the endogenous response results in thus-far irreversible damage to the myocardium². This damage
41 commonly takes the form of cardiac fibrosis, excessive scarring and defunctionalization of the cardiac
42 tissue, which increases risk and mortality of a future cardiac event^{2,3}.

43 Aging is a major risk factor for cardiovascular disease (CVD) and numerous other diseases and is a growing
44 area of research given the aging population in the United States and other countries^{4,5}. Furthermore, data
45 increasingly suggests that age and sex play significant roles in the likelihood and severity of MI and
46 resulting fibrosis⁵⁻⁸. Males over 50 years of age tend to have a higher risk of fibrosis and typically
47 experience MI 9 years earlier than females, differences that subside as age approaches 80 years or

48 greater^{6,9,10}. While the precise reasons for these discrepancies remain elusive, recent data suggests that
49 aging and sex-related long-term changes to the cardiac microenvironment account for the differential
50 response to MI^{6,8,11}.

51 In recent years, the use of extracellular matrix (ECM) or ECM-derived materials in the treatment of cardiac
52 fibrosis has seen reliable success in pre-clinical trials¹²⁻¹⁶. These approaches take advantage of the
53 endogenous cardioprotective effects of ECM on the local microenvironment to promote functional tissue
54 recovery after cardiac injury^{17,18} through local immunomodulation, stem cell recruitment, and decreased
55 scar tissue formation¹⁹⁻²¹. These effects synergize to enhance regenerative healing and decrease fibrosis
56 post-MI. However, the mechanisms by which ECM promotes cardiac repair are not well understood, and
57 recent studies suggest that the release of embedded signaling molecules such as cytokines or growth
58 factors²² and ECM-microRNA (miRNA) interactions¹¹ are major effectors of both pro and anti-fibrotic
59 signaling pathways post-MI.

60 The identification of these particular factors suggest that the beneficial effects of ECM may be conferred
61 by extracellular vesicles (EVs), as both cytokines and miRNAs are commonly packaged in EVs when
62 secreted from cells as opposed to being free-floating²³. Previously unidentified ECM-bound EVs could be
63 key mediators of the beneficial effects of ECM treatment, and isolation, quantification, and
64 characterization of these EVs will elucidate essential mechanisms of ECM-mediated cardioprotection.
65 Furthermore, the isolation of key functional compounds, either EVs themselves or those contained in EVs,
66 may provide the benefits of ECM treatment while mitigating many associated challenges, such as immune
67 response, sample preparation variability, and sustainability of production. Another challenge, however, is
68 how to modulate key regulators of fibrosis-related signaling pathways after identifying them. While
69 cytokine-mediated inflammatory signaling pathways are attractive targets for clinical intervention, as they
70 play a pivotal role in the health and functionality of a tissue and allow for direct intervention in the onset

71 and resolution of inflammation^{24,25}, the degree and mechanisms of involvement remain an active area of
72 research²⁴. Recent advances in our understanding of the tissue microenvironment *in vivo* have suggested
73 that this may be due to targeted paracrine signaling controlling these effects, resulting from the highly
74 specific packaging of miRNAs and cytokines in exosomes, a specific, tightly regulated class of EV²³.

75 Exosomes are a subgroup of EVs with diameters typically between 30 nm and 200 nm that are commonly
76 released from most cell types and contain cytokines, chemokines, miRNA, and other miscellaneous
77 signaling molecules that affect function in recipient cells. These contents influence many diverse and
78 pathologically relevant biological processes, including angiogenesis, immunomodulation, endothelial and
79 epithelial to mesenchymal transition, and cell differentiation, and as such exosomes are both packaged
80 and released from cells in a highly controlled manner^{23,26,27}. As a result, recent interest in exosomes has
81 primarily been in the role of maintaining tissue health through intra-tissue signaling and local
82 immunomodulation^{23,27}. This has been bolstered by the recent discovery of exosome-like EVs embedded
83 in decellularized tissue from several human organs, including the urinary bladder and small intestine²⁶,
84 and decellularized mouse atrium²⁸, as opposed to biofluid-derived EVs which have so far been ubiquitous.
85 These embedded EVs showed beneficial immunomodulatory effects, and those isolated from cardiac
86 tissue enhanced cardiomyocyte function *in vitro*^{28,29}, which provides exciting prospects for how these EVs
87 may affect MI response and subsequent cardiac fibrosis and suggests that these EVs may be a core
88 functional component of biosignaling in the ECM. Further investigation of these EVs may reveal precise
89 mechanisms by which ECM treatment confers protective effects, both furthering knowledge of the
90 interplay between microenvironment and tissue health and providing a wealth of targets for clinical
91 intervention without necessitating the use of ECM. However, the impact of both induced and innate
92 differences in the microenvironment may have on these ECM-bound exosomes is currently unknown.

93 Recently, exosomes have been increasingly investigated for links with MI response¹⁴. Exosomes isolated
94 from the cerebrospinal fluid or plasma of young or aged subjects have been demonstrated to have
95 differential effects on modulation of systemic inflammation and progression of neurodegenerative
96 diseases^{4,30}, and these differences can significantly affect CVD outcomes *in vivo*³⁰. However, despite
97 evidence suggesting that there are functional differences between exosomes from young or aged
98 subjects, there has been little evaluation of the specific differences between these exosome populations.
99 For this reason, exosomes have become an attractive target for ascertaining specific age-related changes
100 in the cardiac microenvironment and the impact of any additional factors.

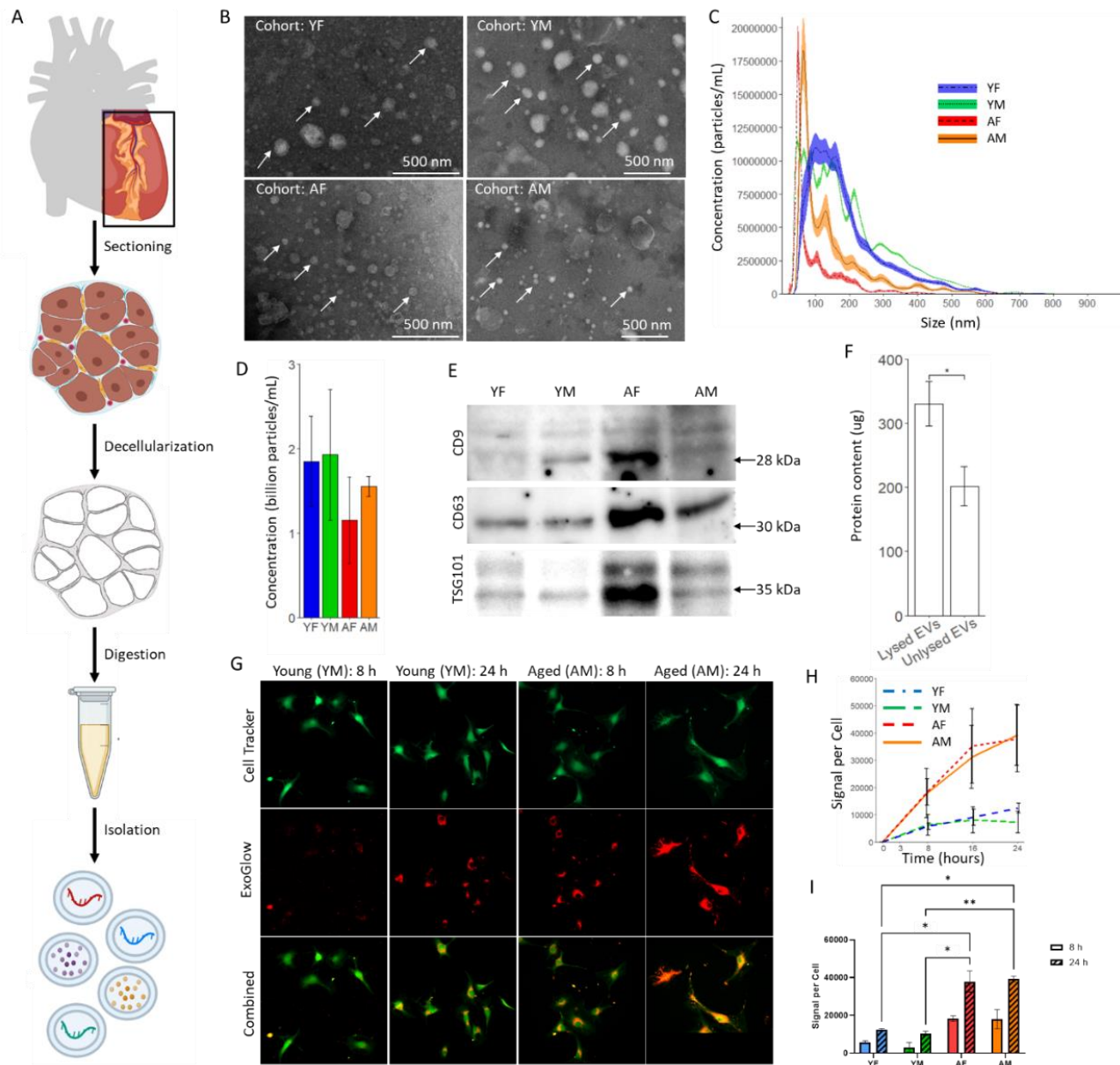
101 In this study we show for the first time in literature the presence of ECM-bound exosome-like EVs in
102 human left ventricular (LV) tissue, and report the changes in size, cytokine content, and miRNA content
103 of these LV vesicles (LVVs) as a function of age and sex. Furthermore, we study the differential effect of
104 LVVs derived from different age and sex groups on the stress response and fibrotic transdifferentiation of
105 cardiac fibroblasts (CFs) to myofibroblasts (MFs) in both human and murine models. Following this, we
106 examine the role of select miRNAs identified from the LVVs in modulating this transdifferentiation. In this
107 way, we suggest that ECM-bound exosomes are a major functional unit of the cardioprotective effects of
108 the ECM, hosting previously identified signaling molecules of interest and recapitulating the effects of
109 ECM treatment on the local microenvironment. Investigating the effects of age and sex on the physical
110 characteristics and composition of human LVVs and how LVVs influence the fibroblast transdifferentiation
111 behavior as a function of age and sex will pave the way for understanding the mechanisms of cardiac
112 fibrosis and developing new treatment strategies to prevent fibrosis and MI.

113 **RESULTS**

114 ***Left Ventricular Vesicle (LVV) Isolation and Characterization:*** Human heart left ventricular tissues were
115 subjected to a detergent-free decellularization and EV isolation process (Figure 1A). Transmission electron

116 microscopy (TEM) imaging verified the presence of EVs in the ECM isolate and demonstrated a stark size
117 difference between young and aged tissue-derived vesicles (Figure 1B). This difference was also observed
118 with nanoparticle tracking analysis (NTA), with aged EVs having average size of $100 \text{ nm} \pm 25 \text{ nm}$ and young
119 EVs having average size of $175 \text{ nm} \pm 25 \text{ nm}$ (Figure 1C). All samples fell primarily within the expected size
120 range for exosomes (30-200 nm), and dispersity decreased in aged tissue-derived samples compared to
121 young. The concentration of vesicles was not significantly different between cohorts (Figure 1D). Western
122 blot was performed to identify characteristic exosome markers CD9, CD63, and TSG101 (Figure 1E). These
123 results showed that the particles were, or contained, exosomes. Lysing these vesicles increased the
124 measured protein content in solution by over 50% (Figure 1F), indicating that the isolated LVVs contained
125 proteins.

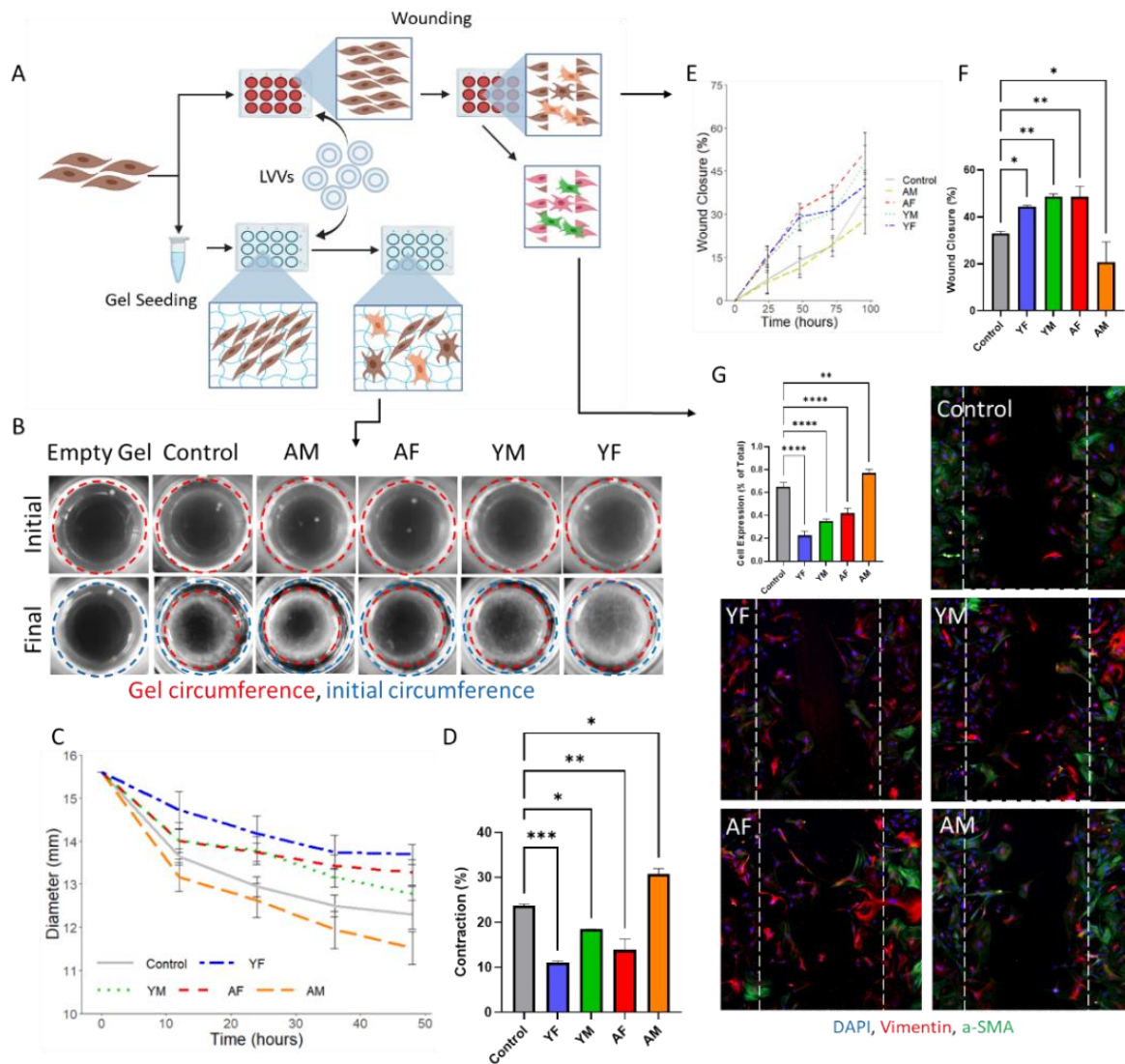
126 ***LVV Uptake by Human Cardiac Fibroblasts (hCFs):*** Uptake of EVs by hCFs was confirmed by tracking
127 stained EVs in cells (Figure 1G). Aged EVs were taken up by hCFs at a nearly 2 times higher rate compared
128 to young EVs (Figure 1H), with a nearly 2x increase in concentration of aged EVs per cell from 8 to 24 h
129 post treatment, and only up to 1.5x increase in concentration of young EVs (Figure 1I). Higher overall
130 quantities of aged EVs per cell were also taken up compared to young EVs, with aged EVs being taken up
131 at 2 to 3 times the quantity of young EVs at all timepoints (Figure 1I).



132
 133 **Figure 1.** Functional Exosomes can be Obtained from Human Left Ventricular Extracellular Matrix with
 134 Distinct Aging-Related Changes. (A) Brief overview of the ECM-bound EV isolation process. (B)
 135 Transmission electron microscopy for representative imaging of all four cohorts. (C) Nanoparticle tracking
 136 analysis with error area of EVs from all four cohorts. (D) Typical concentration of LVV per sample. (E)
 137 Western blotting of lysed LVV showing the characteristic exosome markers. (F) Protein encapsulation
 138 within LVV. (G) Representative images of stained EV uptake by hCFs, with corresponding (H) uptake rate
 139 and (I) overall uptake by cells ($n \geq 3$ for both LVV sources in all cohorts, 5 images per sample). Data are
 140 presented as the mean \pm standard deviation. * $p < 0.05$, ** $p < 0.01$, assessed by Student's t-test with
 141 Welch's correction for (D), (F), and (I).

142 **Effect of LVVs on 3D hCF Gel Contraction:** To assess the effects of LVV treatment on myofibroblast
143 transdifferentiation in 3D culture, hCFs were seeded either in collagen gels with gel contraction assessed,
144 or on tissue culture plates with wound healing (through scratch assay) assessed (Figure 2A). For gel
145 contraction assay, cells were evenly distributed throughout the gel during seeding and attached and
146 spread within the gels (Supplemental Figure S1). All gels maintained structural stability for at least 48 h
147 and no contraction was observed in the cell-free gel control (Figure 2B). The size of the cell-loaded gels
148 from all groups followed a logarithmically decaying curve over time and, compared to the LVV-untreated
149 control, the reduction in gel size was decreased after treatment with young-female (YF), aged-female (AF),
150 or young-male (YM) LVVs and increased after treatment with aged-male (AM) LVVs (Figure 2C). The total
151 contraction after 48 h was significantly higher in the AM LVV treated group, and significantly lower in the
152 YF, AF, and YM LVV treated groups, compared to the untreated control (Figure 2D). The least contraction
153 was observed with AF group.

154 **LVVs Affect hCF Wound Healing and Transdifferentiation:** Scratch assay demonstrated 1.5 or 2 times
155 enhanced wound closure over culture period after treatment of hCFs with YF, AF, and YM LVVs compared
156 to the control, and 30% decreased wound closure after treatment with AM LVVs (Figure 2E). At the
157 endpoint, all groups demonstrated significantly different wound closure behavior from the control, with
158 AM LVVs having decreased closure while other groups having increased it (Figure 2F). A similar trend was
159 observed with rat CFs (Supplemental Figure S2), although YF LVVs showed no beneficial effects on these
160 cells. No group achieved full wound closure in the time allotted, with the YF, AF, and YM groups achieving
161 >45% average closure, the control achieving ~37% closure, and the AM group achieving <30% closure
162 (Supplemental Figure S3). Immunostaining of cells at 96 h post treatment revealed significant differences
163 in α -SMA expression between all groups and the control, with the YF, AF, and YM groups showing <40%
164 α -SMA expression compared to ~65% expression in the control and >75% expression in the AM group

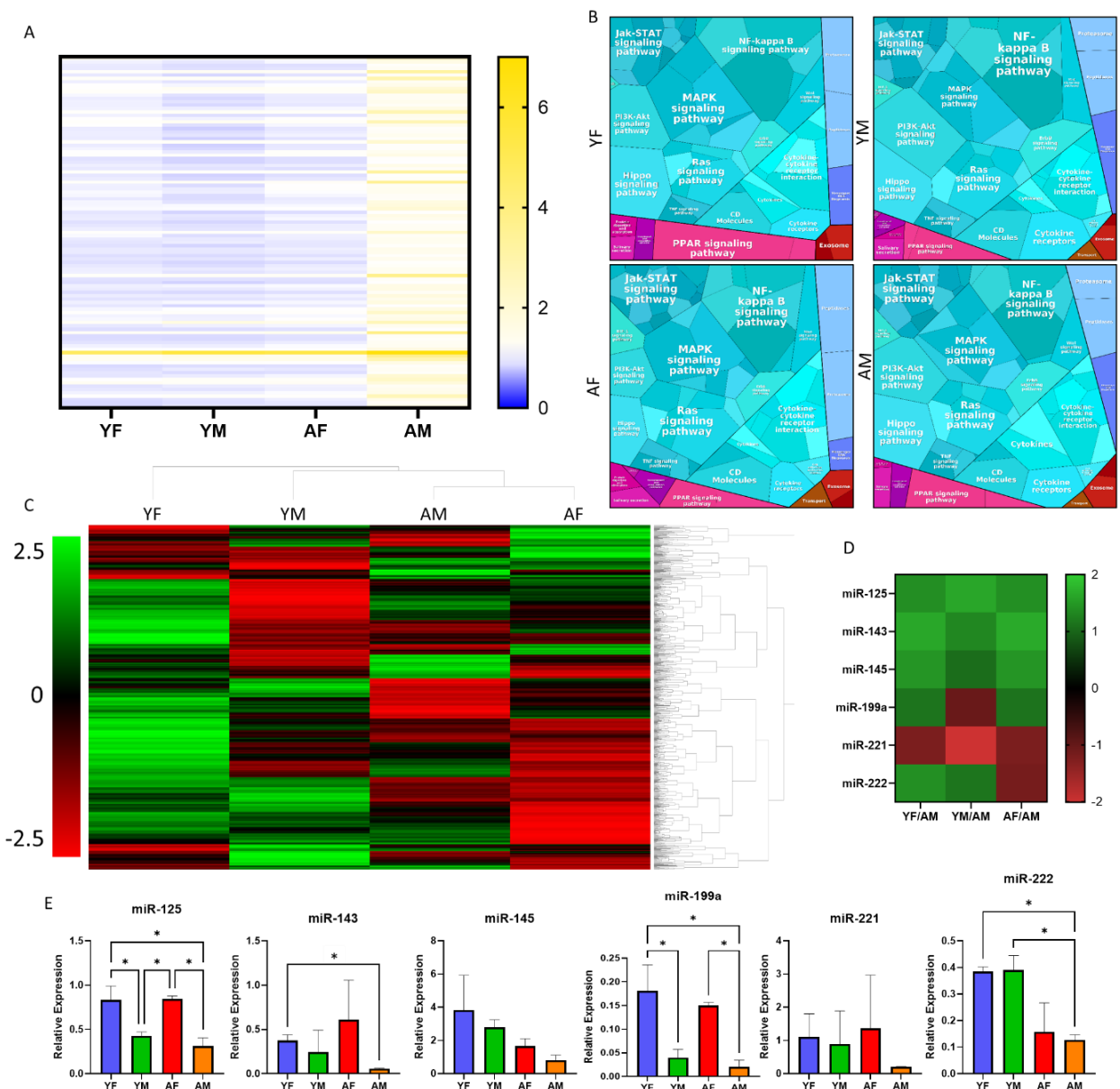


165
 166 **Figure 2.** LVVs Modulate Fibroblast Behavior In Vitro to Control Transdifferentiation and Fibrotic Effects.
 167 (A) Schematic briefly showing the assays performed with LVV treatment and resulting data. (B)
 168 Representative images of gels for both baseline and final timepoints for each cohort with gel
 169 circumference indicated, quantified as rate of gel contraction over 48 h (C) and final contraction
 170 percentage calculated relative to initial gel diameter (D) for each cohort ($n \geq 3$ for both LVV sources in all
 171 cohorts). Wound closure (E) rate and (F) percentage over 96 h for each cohort ($n \geq 3$ for both LVV sources
 172 in all cohorts, 2 technical replicates per sample, 3 images per replicate, for 2 independent repetitions). (G)
 173 Percentage of cells expressing α -SMA for each cohort, and representative images of stained wound area
 174 ($n \geq 3$ for both LVV sources in all cohorts, 3 images per sample). Data are presented as the mean \pm standard
 175 deviation. * $p < 0.05$, ** $p < 0.01$, *** $p < 0.001$, assessed by one-way ANOVA with Tukey's post-hoc for
 176 (D), (F), and (G).

177 (Figure 2G). The differences observed inversely corresponded to wound healing capacity, with groups
178 demonstrating enhanced wound healing capacity expressing lower levels of α -SMA and vice-versa
179 (Figures 2F and 2G). Greater than 95% of cells in all groups expressed vimentin, confirming them as
180 fibroblasts (Supplemental Figure S4).

181 **Profiling of Cytokine Content:** Cytokine profiling via dot blot-based immunoassay revealed differential
182 concentrations of cytokines present in LVVs from different subject groups. In general, when compared to
183 YF LVVs, which had the measured lowest quantity of cytokines (Supplemental Figure S5), YM and AF LVVs
184 showed little difference while AM LVVs showed over 3-fold higher levels of several cytokines (Figure 3A).
185 These include Angiopoietin-2 (2.99-fold), Dkk-1 (2.58-fold), Emmprin (2.455-fold), IFN- γ (2.84-fold), IL-1 α
186 (3.05-fold), Kallikrein-3 (3.31-fold), and SDF-1 α (2.94-fold) among others (Supplemental Table S1).
187 Proteomapping of the affected KEGG pathways showed upregulation of transport and HIF-1, Ras, and TNF
188 signaling, and downregulation of PPAR signaling in aged subjects compared to young, and in males
189 compared to females (Figure 3B). Interestingly, cytosolic DNA sensing was observed in males but not
190 females. Additionally, gene ontology analysis showed that cytokines present in the AM LVVs were
191 associated with regulation of tissue remodeling, positive regulation of receptor-mediated endocytosis and
192 cytokine production, and negative regulation of cell death and wound healing (Supplemental Table S2).
193 Only male LVVs were involved in negative regulation of wound healing (Supplemental Table S2).

194 **Identification of miRNA Content:** miRNA profiling via Nanostring analysis revealed highly upregulated
195 exosomal miRNA populations in both young groups relative to both aged groups (Figure 3C). Interestingly,
196 many of the miRNAs upregulated in YF, YM, and AF LVVs were downregulated in the AM group. From the
197 over 800 miRNAs profiled, six were identified as both exosomal and cardioprotective from literature³¹⁻³⁴,
198 although the activities of these miRNAs have been primarily characterized for cardiomyocytes. Of these
199 six, five were upregulated in other groups relative to AMs (Figure 3D). RT-qPCR revealed that four were

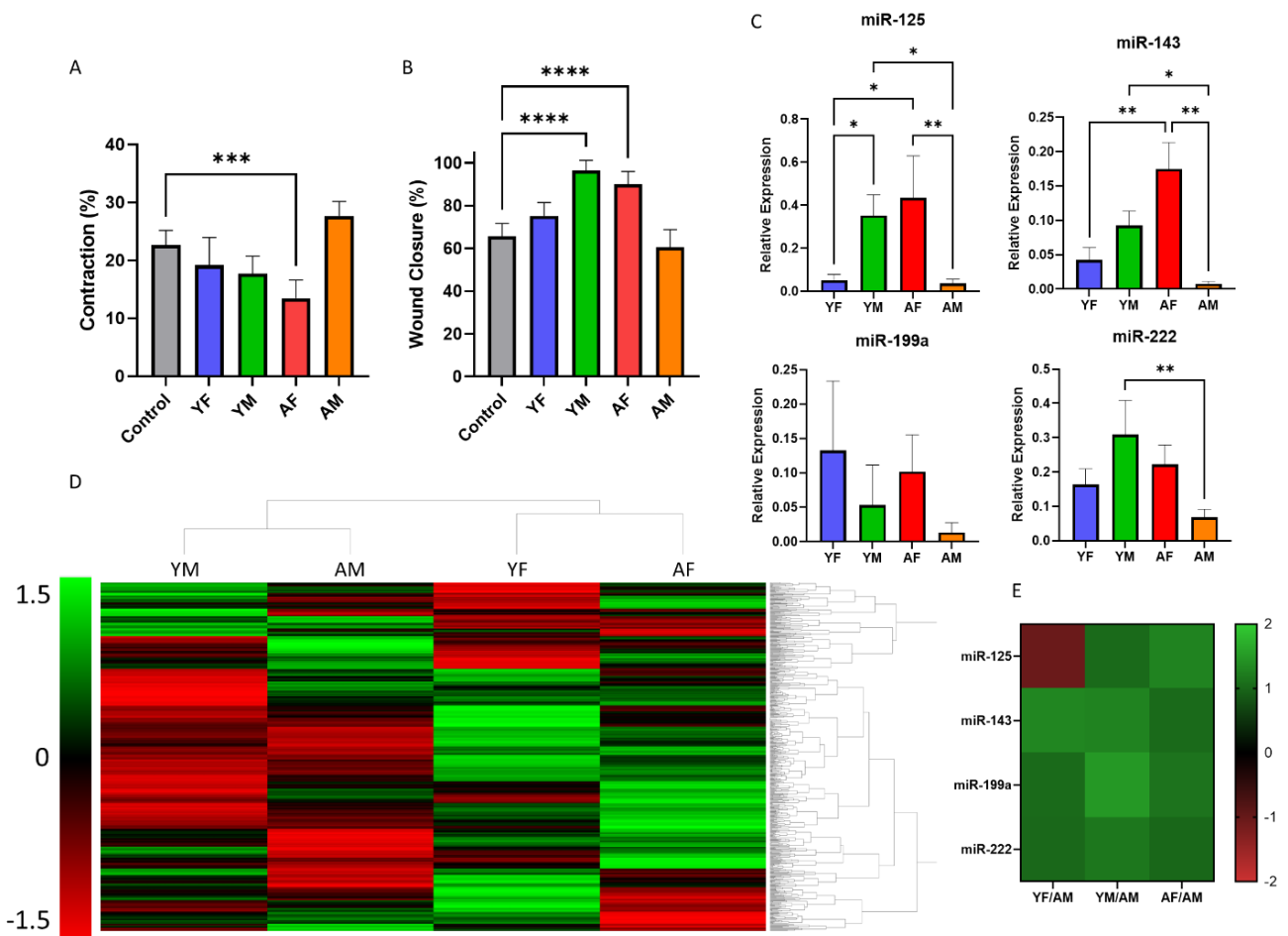


200
 201 **Figure 3.** Left Ventricular Vesicles (LVVs) Affect a Wide Variety of Aging and MI-Related Pathways
 202 Depending on Age and Sex. (A) Heat maps showing the cytokines detected in each cohort relative to the
 203 internal positive control. For read data, see Supplemental Table S1. (B) Proteomaps showing the KEGG
 204 pathways affected in response to the cytokines in each cohort. (C) Heatmap showing the full miRNA
 205 profiling for each biological replicate of each cohort. (D) Nanostring results for the 6 identified exosomal
 206 miRNAs from literature, for each cohort relative to AM. (E) PCR results for the identified miRNAs. Data are
 207 presented as the mean \pm standard deviation. * $p < 0.05$, assessed by one-way ANOVA with Tukey's post-
 208 hoc for (E).

209 significantly increased in at least one comparison against AM (Figure 3E). Interestingly, miR-125 and miR-
210 199a were elevated in both female groups compared to both male groups, while miR-143 was decreased
211 only in AM LVVs. Additionally, miR-222 was elevated in young groups compared to aged. Both miR-145
212 and miR-221 showed no significant differences between any groups, which was unexpected as these
213 miRNAs are often considered as conjugated units with miR-143 and miR-222, respectively.

214 ***Features of LVVs are Recapitulated in Mouse Models:*** Preliminary results had shown that LVV effects
215 were mostly consistent between human and rat models (Figure 2F, Supplemental Figure S2), so a more
216 controlled mouse study was conducted to further validate these results and account for the biological
217 variability and difficulty of obtaining additional human samples. Mice (n=6) were similarly categorized as
218 YF, YM, AF, or AM (Supplemental Table S3). The collagen contraction assay using mouse LVVs (mLVVs) and
219 mouse CFs (mCFs) showed a similar trend to that observed from human samples, but both young groups
220 showed no improvement compared to the untreated control, and the AM group showed no significant
221 increase in contraction in the same comparison (Figure 4A). However, the AF-treated group showed a
222 significant decrease in contraction compared to the control, and YF, YM, and AF groups showed a
223 significant decrease in contraction compared to the AM group. The results from the wound healing assay
224 followed this trend, and YM and AF, but not YF or AM, were significantly different from the control (Figure
225 2B). However, once again the YF, YM, and AF groups showed significantly increased wound healing
226 compared to the AM group. These results echo the preliminary results obtained from rat models
227 (Supplemental Figure S2).

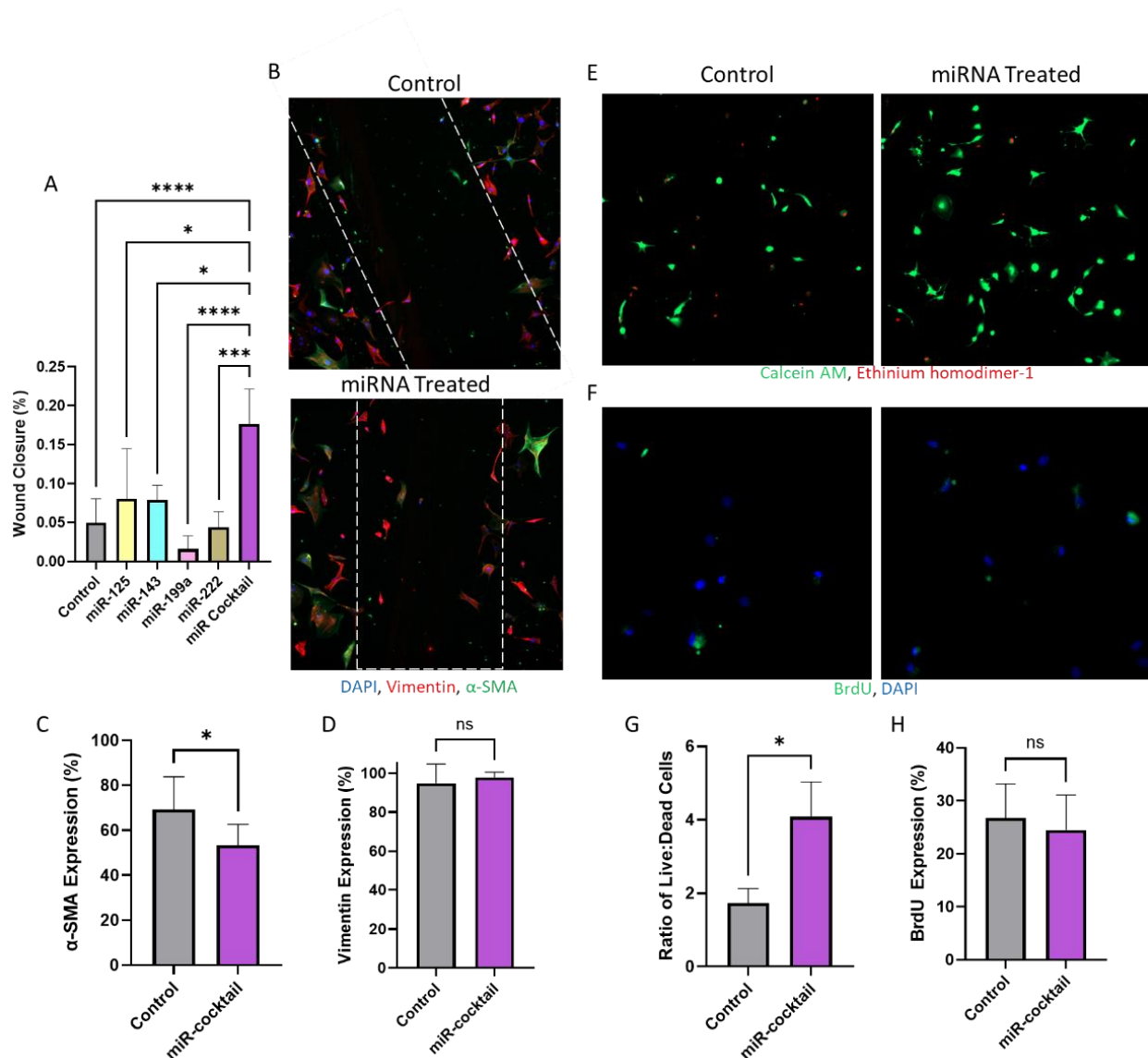
228 Also assessed in mLVVs was the relative expression of the target miRNAs, excluding those which showed
229 no significance in human samples. First these four targets were measured by RT-qPCR (Figure 4C). Three
230 of the four targets showed significantly increased expression in at least one group compared to the AM
231 cohort, with miR-199a demonstrating no significant difference between any groups. Additionally, the



232
 233 **Figure 4.** Validation of Trends in Human LVVs in Mouse Cardiac Model EVs. (A) Gel contraction over 48 h
 234 for collagen hydrogels, as a percentage of initial gel diameter (n = 6 biological replicates for each cohort,
 235 for 2 independent repetitions). (B) Wound closure over 60 h, as a percentage of initial wound area (n = 6
 236 biological replicates for each cohort, for 2 independent repetitions). (C) PCR results for the 4 miRNAs
 237 selected from human LVVs (n = 3 biological replicates, each pooled from 2 separate hearts' miRNA, for 2
 238 independent repetitions). (D) Heatmap showing the full miRNA profiling for each replicate used for PCR
 239 (each replicate is from 2 separate hearts' isolated miRNA) and (E) a heatmap for each cohort for the 4
 240 selected miRNA targets (from the data presented in the full profiling). * p < 0.05, ** p < 0.01, *** p <
 241 0.001, **** p < 0.0005, assessed by one-way ANOVA with Tukey's post-hoc for (A), (B), and (C).

242 trends in miRNA expression slightly differed between mouse and human LVVs. This difference can likely
243 be attributed to innate differences in mouse and human physiology and native response to cardiac
244 insult, which may be fundamentally different³⁵. Nevertheless, the AM group still showed the lowest
245 expression of all four target miRNAs, and that, with the decreased in some miRNA expression observed
246 from the YF group, is co-concurrent with mitigated benefits in contraction and wound healing. Full miRNA
247 profiling of the mLVVs was also performed (Figure 4D). There was a higher overall upregulation of miRNAs
248 in both female groups compared to both male groups. Interestingly, among upregulated miRNAs there
249 was notable overlap between the YM and AF groups, although this overlap also commonly includes the
250 YF or AM groups. The 4 selected target miRNAs pulled from the total profiling were mostly consistent with
251 the RT-qPCR results, although for the YF group miR-125 showed downregulation compared to the AM
252 group (Figure 4E).

253 ***miRNAs Partially Recapitulate LVV Effects:*** To study the effect of miRNAs on wound closure, cells were
254 treated with miR-125, miR-143, miR-199a, or miR-222 mimics, or a cocktail containing all four. No
255 significant differences were observed from treatment with individual miRNAs, although some increase in
256 wound healing was detected after treatment with miR-125, while the miRNA cocktail-treated groups
257 demonstrated up to three-fold greater wound closure compared to the scramble siRNA-treated control
258 over the culture period (Figure 5A). At 48 h, the miR cocktail-treated cells had healed significantly more
259 than scramble siRNA treated control cells. Staining of the cells (Figure 5B) revealed a significant decrease
260 in α -SMA expression of the treated cells compared to control (Figure 5C) with no change in vimentin
261 expression (Figure 5D), as was observed with LVV treatment. Quantification of Live/Dead staining (Figure
262 5E) and BrdU staining (Figure 5F) of hCFs subjected to MI-like conditions (3 h hypoxia) showed about a
263 2.5-fold increase in the ratio of live cells to dead cells after treatment with miRNA cocktail compared to
264 control cells (Figure 5G), while relative BrdU expression was similar between both groups (Figure 5H).



265
 266 **Figure 5.** miRNA Treatment Partially Recapitulates LVV Effect *in vitro*. (A) Final timepoint wound closure
 267 percentage of control and miRNA-treated groups ($n \geq 3$, 2 technical replicates per sample, 3 images per
 268 replicate). (B) Immunostaining showing expression of DAPI (blue), α -SMA (purple), and vimentin (green)
 269 for control or miRNA-treated hCFs post-healing. Quantification of local expression of α -SMA (C) and
 270 vimentin (D) as a percentage of total cells observed. Representative images showing (E) live/dead stain or
 271 (F) BrdU stain following MI-like hypoxia treatment of control or miRNA-treated cells ($n \geq 3$, 3 images per
 272 sample). Quantification of (G) live/dead or (H) BrdU assay. Data are presented as the mean \pm standard
 273 deviation. * $p < 0.05$, assessed by ANOVA with Tukey's post-hoc for (A), and Student's t-test with Welch's
 274 correction for (C), (D), (G), and (H).

275 **DISCUSSION**

276 In this study, we isolated and characterized the matrix-bound vesicles in left ventricular tissues of young
277 (19-29 years old) and aged (51-63 years old) male and female human donors and assessed their effect on
278 cardiac fibroblast transdifferentiation through measurement of contractility, wound healing, and α -SMA
279 expression. Interestingly, we found differences in size distribution, uptake, and cytokine and miRNA
280 profiles between aged and young LVVs, as well as male and female LVVs. LVVs from aged hearts were
281 smaller in size than those from young, and were taken up more rapidly by cells. Additionally, LVVs from
282 all cohorts expressed common exosome markers, showing that at least some of the isolated LVVs were
283 exosomes. Cytokine content was higher in LVVs from aged tissues compared to young, and in males
284 compared to females, with the highest content observed in AM LVVs. Conversely, the lowest miRNA
285 content was observed in AM LVVs. While LVVs from females contained more miR-125 and miR-199a than
286 LVVs from males, those from young tissues contained more miR-222 than aged. Remarkably, hCFs
287 embedded in collagen gels showed increased contraction upon treatment with AM LVVs compared to
288 untreated controls, and decreased contraction when treated with LVVs from other groups. Similarly, *in*
289 *vitro* scratch assay showed decreased wound closure in AM LVV treated cells compared to untreated
290 controls and increased closure in cells treated with other LVVs groups in both human and murine cell lines.
291 Immunostaining of cells post-scratch assay showed higher α -SMA expression in AM LVV-treated cells than
292 the control, and lower expression in other groups. Repetition of the scratch assay using miRNA treatment
293 instead of LVVs showed that miRNA cocktail treatment, but not individual miRNAs, could recapitulate
294 these effects. Remarkably, treatment with this cocktail showed a protective effect on hCFs subjected to
295 MI-like conditions, significantly decreasing cell death without significantly affecting proliferation. These
296 results show for the first time that matrix bound EVs in the left ventricle change in size, content, and

297 bioactivity in an age- and sex-dependent manner, and that AM LVVs may play a novel and pivotal role in
298 chronic pro-fibrotic cardiac signaling.

299 In this study we showed for the first time the presence of exosome-like EVs in human left ventricles and
300 characterized their size and characteristics as a function of age and sex. Interestingly, although EVs from
301 all cohorts were in the size range of exosomes (30-200 nm)³⁶, both young groups showed greater size and
302 dispersity than both aged groups despite similar concentrations and measured quantity isolated. These
303 data suggest that there is a physical difference between the LVVs present in aged ECM compared to young
304 ECM. It is established that cell uptake of vesicles is size-dependent for exosomes³⁷, so this may suggest a
305 need for more rapid uptake of these exosomes for expedited response in older, more “at risk” hearts.
306 Alternatively, the production of smaller vesicles may result from increased vesicle specialization in aged
307 tissue^{23,27}, although this does not explain the increased cytokine content observed in the AM LVVs. In
308 either case, these data suggest substantial differences in exosome uptake and secretion mechanics
309 between young and aged hearts. While the smaller, aged tissue EVs were taken up more rapidly and to a
310 greater degree than young tissue EVs, anti-fibrotic effects were mostly conferred by young LVVs. This
311 suggests that the miRNA-mediated effects conferred by young EVs are not intended for a rapid response
312 or may not be highly dose-dependent. Alternatively, the detrimental effects observed from AM LVVs
313 might result from their high cytokine content. These findings suggest a different core paracrine response
314 to cardiac injury between young and aged, and male and female myocardium which has not been
315 previously described in literature.

316 A general upregulation of most assessed cytokines was observed in AM LVVs compared to other cohorts,
317 as was expected based on available data for sex³⁸ and age³⁹ dependence of cytokine profiles. Cytokines
318 related to pro-fibrotic processes post-MI and other detrimental cardiac processes were present in greater
319 amounts in AM LVVs compared to other cohorts. While the AM cohort demonstrated the highest

320 upregulation of inflammatory cytokines, both aged groups showed some upregulation of cytokines such
321 as VCAM-1 and IL-1 β (Supplemental Table S1), which are involved in further injury or fibrosis post-MI^{40,41}.
322 These data suggest that AM LVVs may participate in microenvironment-driven inflammaging, which has
323 been suggested as a major contributor to cardiac fibrosis⁴². Some other cytokines elevated in AM LVVs,
324 such as IFN- γ , MMP9, and myeloperoxidase, which are involved in cardiometabolic dysfunction⁴³ and
325 fibrotic remodeling post-MI⁴⁴⁻⁴⁶, also suggest that this contribution is greater from AM LVVs, and that AM
326 LVVs may more directly contribute to long-term cardiac damage from the microenvironment.
327 Interestingly, AM LVVs also demonstrated greater levels of cardioprotective cytokines than other cohorts.
328 This may be due to endogenous ischemic preconditioning, which has been suggested to be mediated by
329 atypical cytokine interactions⁴⁷⁻⁵⁰. Since neither AM subject suffered from CVD or other diseases which
330 may affect the heart microenvironment or died from a heart-related cause, the observed high levels of
331 cytokines may be a result of ongoing endogenous preconditioning. In fact, the AM group demonstrated
332 increased GM-CSF and GDF-15, SDF-1 α , and TNF- α , which have been identified as major signaling
333 molecules in ischemic preconditioning^{48,51}. Overall, AM demonstrated the greatest expression of both
334 damaging and protective cytokines.

335 A different trend was observed from miRNA analysis of six cardioprotective miRNA, with AM consistently
336 demonstrating the lowest expression of all miRNAs assayed. This was apparent in the full miRNA profiling,
337 where YF LVVs show the most consistent upregulation of miRNAs and AM LVVs show the most consistent
338 downregulation of miRNAs, for all 800+ miRNAs assessed. Based on this trend, potential miRNA targets
339 were identified by comparison of expression levels relative to AM expression to find the largest
340 upregulation. First, targets were selected from literature and validated using the profiling data, then
341 quantified using RT-qPCR. The targets were as follows: miR-125, shown to protect against ischemic and
342 reperfusion injury^{32,52}, was significantly increased in female tissue LVVs in both aged and young subjects.

343 miR-199a, a cell survival promoter and key regulator of the endothelial nitric oxide pathway^{31,32}, was
344 significantly increased in AF LVVs compared to both male groups. These data suggest a shift in miRNA
345 production may be integral to differences in response to cardiac event between males and females. While
346 miR-143, implicated in regulation of cardiac regeneration and protective against carotid injury^{53,54}, was
347 significantly increased in YF LVVs compared to AM, this may result from a combination of age and sex
348 differences. Additionally, miR-222 was age-dependent, while miR-145 and miR-221 showed no significant
349 difference between any groups. This is an interesting result particularly because miR-143 and miR-145,
350 and miR-221 and miR-222 are often considered as conjugated pairs rather than individual miRNAs³².

351 Cell assays were selected to determine relative transdifferentiation of CF samples treated with the same
352 concentration of LVVs from each group. These provided metrics of contractility, which is enhanced in
353 MFs^{40,55}, proliferation and proliferative wound healing, which are decreased in MFs^{55,56}, and expression of
354 characteristic MF marker α -smooth muscle actin (α -SMA)⁴⁰. These data show that LVVs from the AM
355 cohort tended to promote MF-like behavior from cells in both 2D and 3D culture. This is an interesting
356 result, as existing literature suggests that the application of ECM in general tends to promote a reparative,
357 anti-fibrotic microenvironment in the myocardium¹⁷⁻¹⁹. While these anti-fibrotic effects are still observed
358 from AF LVVs and both young LVV groups, this is not the case for AM LVVs, suggesting that AM LVVs
359 contain distinctly pro-fibrotic factors. This observation aligns with expected effects from heart tissue
360 subjected to inflammaging effects⁴². Furthermore, this is supported by additional preliminary data on rat
361 cardiac fibroblasts as well as well-controlled trials with mouse cardiac fibroblasts. In both cases, both the
362 YM and AF groups demonstrated beneficial effects consistent with the human trials, while the AM group
363 demonstrated pro-fibrotic effects to a comparable degree as direct TGF- β treatment in the rat model. In
364 the mouse model, the AM group was significantly detrimental compared to all other treatment groups,

365 further suggesting that some aspect of AM LVVs is inducing pro-fibrotic effects in direct opposition to
366 other cohorts in this study.

367 Further investigation of AM LVV factors may implicate novel targets for therapeutic intervention of aging-
368 related inflammatory pathways which stimulate cardiac fibrosis. Remarkably, however, the AF, YM, and
369 YF LVVs exhibited anti-fibrotic effects, similar to what has been observed from treatment with
370 decellularized ECM¹⁷⁻¹⁹. Of these, the YF group demonstrated the greatest reduction in contractility and
371 α -SMA expression, while AF LVVs promoted the greatest increase in wound healing. This is an interesting
372 result, as LVVs from the female subjects displayed the greatest anti-fibrotic behavior overall, consistent
373 with clinical outcomes for the onset of fibrosis. Together, these findings suggest that the beneficial effects
374 of LVVs are sex and age-dependent, and that LVVs can recapitulate the beneficial effects of ECM or
375 introduce pro-fibrotic factors depending on these conditions. Further investigation of these differences
376 will help elucidate the mechanistic reason for the clinically observed importance of sex and age in the
377 onset of cardiac fibrosis.

378 To better understand these mechanisms, we attempted to recapitulate the effects of LVV treatment by
379 transfecting hCFs with the identified miRNAs of interest: miR-125, miR-143, miR-199a, and miR-222. While
380 transfection with individual miRNAs did not yield significant results, treatment with a combination of all
381 four miRNAs enhanced wound healing and survivability and decreased transdifferentiation of hCFs,
382 similarly to treatment with LVVs. Most interestingly, this miRNA cocktail exhibited these same effects
383 under MI-mimicking conditions. Treatment more than doubled cell survivability after 3 hours of MI
384 compared to the control while cell proliferation was nearly unchanged, suggesting that the synergistic
385 effects of these miRNAs not only reduce damage from CVD events but also promote survival and
386 “reparative” signaling. This is an exciting result, and indicates that novel synergistic effects of exosomal
387 miRNAs can both inhibit the onset of cardiac fibrosis and protect cells from MI-induced cell death through

388 endogenous pathways, although further targets must be identified to better recapitulate the full effects
389 of LVV treatment. Similar to how the application of mesenchymal stem cell exosomes can recapitulate the
390 cardioprotective effects of the source cells^{14,57}, the isolation of key cardioprotective agents, such as
391 exosomal miRNA combinations, from the ECM may allow for enhanced treatment options. By
392 investigating key differences observed between the AM LVVs and other cohorts and common factors
393 between AF, YM, and YF LVVs, the mysteries of the myocardial microenvironment in MI and cardiac
394 fibrosis will be elucidated.

395 In that vein, given the success of treatment with only four miRNAs, we have identified 37 additional
396 targets for either application or inhibition based off the miRNA profiling data (Supplemental Table S4).
397 Specifically, 14 targets are exosomal miRNAs that display similar elevated expression against the AM
398 group to the selected targets, while the remaining 23 are miRNAs that are elevated in the AM group
399 compared to others. While above we have established the benefits of utilizing a synergistic cocktail of
400 miRNAs, other single-miRNA studies have suggested that some miRNAs may also be driving factors behind
401 the pro-inflammatory signaling and other microenvironment changes observed in the heart⁵⁸ and
402 profibrotic changes observed in other organs⁵⁹.

403 In this study we showed, for the first time, the presence of matrix bound exosome-like EVs in the human
404 left ventricle, characterized the physical properties and cytokine and miRNA contents of these LVVs as a
405 function of age and sex, and investigated the effects of these LVVs on cardiac fibroblast
406 transdifferentiation. While recent studies have identified the therapeutic effects of young plasma-derived
407 exosomes^{60,61}, this study is among the first to directly compare exosomes from young and aged subjects,
408 an identified gap in knowledge regarding exosome studies^{4,30}, and is the first to do so with exosomes
409 derived from cardiac tissue. Additionally, this study contributes to understanding of exosome behavior in
410 healthy hearts, which is understudied compared to the knowledgebase for exosomes from hospitalized

411 subjects³⁰. Furthermore, this study reveals previously undescribed synergistic effects of exosomal miRNAs
412 in the progression of cardiac fibrosis and MI-induced damage to cardiac fibroblasts. This study expands
413 the knowledgebase of changes in exosome behavior related to cardiac health during aging, and
414 contributes to the identification of factors involved in cardiac fibrosis and MI and subsequent
415 development of therapeutics that can mitigate or prevent these phenomena.

416 In conclusion, functional exosomes can be found embedded within the ECM of human left ventricular
417 tissue, differing from exosomes traditionally isolated from biofluids. These novel left ventricular vesicles,
418 or LRVs, contain varying quantities of cytokines and miRNA depending on sex and age, with LRVs from
419 aged male subjects showing signs of inflammaging, ischemic preconditioning, and decreased
420 cardioprotective miRNAs. Treatment of fibroblasts revealed that LRVs from aged males tend to promote
421 a pro-fibrotic response, whereas LRVs from females and young males promote an anti-fibrotic response.
422 These data suggest that ECM-embedded vesicles play a crucial role in response to cardiac injury and may
423 be responsible for some cardioprotective effects observed with ECM treatment. Furthermore, these
424 effects were also observed upon treatment of hCFs with a cocktail of cardioprotective miRNAs identified
425 from the LRVs: miR-125, miR-143, miR-199a, and miR-222. This cocktail promoted cell survival under MI-
426 like conditions *in vivo* while partially recapitulating the wound healing effects observed from LRVs. This
427 suggests that miRNAs can mimic the effect of exosomes and possibly be used as therapeutic agents for
428 cardiac fibrosis. However, it should be noted that physical and content characterization of the exosome
429 populations was limited by the small number of human biological replicates available. With only two
430 human subjects from each cohort, it is possible that significant effects were overlooked in this study and
431 internal variability was exacerbated. Nevertheless, further study of these interactions will enhance
432 understanding of the mechanisms by which cardiac injury response occurs and provide novel means for
433 intervention.

434 **METHODS & MATERIALS**

435 ***Tissue Preparation:*** Human heart tissue was collected from donors whose hearts were deemed unsuitable
436 for transplantation through the Indiana Donor Network. IRB approval was waived, as no identifying
437 information was provided by the Indiana Donor Network. All tissue collection was performed in
438 accordance with the declaration of Helsinki. Subjects were selected such that cardiac event or
439 cardiovascular disease was not the primary cause of death. Tissue samples consisted of young female (YF),
440 young male (YM), aged female (AF), and aged male (AM) subjects (N = 2 for each group), where subjects
441 over 50 years old were considered “aged”, and those below 30 years old were considered “young”.
442 Samples were stored at -80 °C prior to sectioning. While still frozen, extraneous fat and connective tissue
443 were excised. Tissue was thawed in sterile PBS at 4 °C and sectioned. Sections with approximately the
444 same surface area and thickness (<300µm) were processed.

445 Mouse heart tissue was collected from C57BL/6J mice (The Jackson Laboratory) according to IACUC
446 guidelines (protocol number: 18-05-4687) with the approval of the University of Notre Dame. Male and
447 female mice were categorized as young (16 weeks old) or aged (72 weeks old), corresponding to the ages
448 of the collected human samples (Supplementary Table S1), with each group having n = 12 samples per
449 group (N = 48 total mice). Mice were euthanized via CO₂ and the whole mouse heart and other tissues
450 were immediately harvested. All mice showed no cardiovascular abnormalities upon death or tissue
451 isolation. Following collection, the left ventricle of the hearts were isolated and immediately processed.

452 ***Decellularization:*** Decellularization and digestion were performed in accordance with current standards
453 for maintaining EV integrity^{62,63}. Tissue sections were agitated in a solution containing peracetic acid
454 (Sigma Aldrich, USA) (0.1%) and ethanol (Sigma Aldrich) (4%) at 200 rpm for 2 h, then in phosphate
455 buffered saline (PBS) at 200 rpm for 2 h, and then again in peracetic acid/ethanol solution at 200 rpm for

456 16 h. Decellularized matrix sections were then washed extensively in PBS and sterile water, blotted on a
457 tissue paper, and frozen at -80 °C.

458 **Decellularized Matrix Digestion:** Frozen heart matrices were lyophilized overnight and ground into a
459 powder using liquid nitrogen and pre-chilled mortar and pestle. ECM powder (200 mg) was then
460 transferred to 1.5 mL microcentrifuge tubes, suspended in 1 mL of digestion buffer containing 0.1 mg/mL
461 collagenase type II (Corning), 50 mM Tris buffer (Sigma Aldrich), 5 mM CaCl₂ (Amresco), and 200 mM of
462 NaCl (Sigma Aldrich), and was mixed vigorously to ensure complete resuspension. The mixture was stored
463 statically at room temperature (RT) for 24 h or until few or no solid particles could be observed in the
464 solution, with brief remixing every 6-8 h.

465 **Vesicle Extraction and Isolation:** Digested matrix solution was centrifuged three times at 500g for 10 min,
466 2500g for 20 min, and 10,000g for 30 min, and the pellet discarded after each centrifugation step to
467 remove any remaining insoluble matrix remnants. The final supernatant was centrifuged at 100,000g at
468 4°C for 70 min using an ultracentrifuge (Optima MAX-XP Tabletop Ultracentrifuge, Beckman Coulter). The
469 pellet was either used immediately or stored dry at -80°C.

470 **Transmission Electron Microscopy:** Single pellets were fixed in 2.5% glutaraldehyde at RT in the dark, then
471 loaded onto plasma-cleaned Formvar/carbon-coated copper 200 mesh grids (Polysciences) and negative-
472 stained with Vanadium staining solution (Abcam, ab172780). Samples were imaged at 80 kV with a TEM
473 (JEOL 2011, Japan).

474 **Nanoparticle Tracking Analysis:** Single pellets were resuspended in 1mL of sterile, particle-free PBS and
475 measured using a NanoSight NS300 machine (Malvern Panalytical) and NTA software version 3.2.16. This
476 method obtains the hemodynamic diameter and concentration of nanoparticles with diameters from 10-

477 1000 nm in solution via Brownian motion analysis. Samples were kept at 4 °C until measurement, and
478 measurements were taken at RT.

479 **Western Blot:** To retain maximum protein blot clarity, decellularization and matrix digestion were
480 performed at 4°C. The pellets were lysed in RIPA buffer containing 1% proteinase inhibitor cocktail (Brand,
481 Country) at 4°C for 30 minutes, then protein concentration was assessed via bicinchoninic acid (BCA) assay
482 (Pierce Chemical). Equal amounts of protein were separated by 12% SDS-PAGE and transferred to blotting
483 membranes, which were incubated overnight at 4°C with the rabbit polyclonal primary antibodies against
484 CD9 (Abcam, ab223052), CD63 (Abcam, ab216130), TSG101 (Abcam, ab30871), and Syntenin-1 (Abcam,
485 ab19903) at (1:1000) dilutions, and against GRP94 (Abcam, ab3674) at 1:2000 dilution, then for 1 h at RT
486 with HRP-conjugated goat anti-rabbit secondary antibody (Abcam, ab205718). Membranes were then
487 exposed to a chemiluminescent substrate (Clarity ECL, Bio-Rad) and imaged using a ChemiDoc-It2 imager
488 (UVP, Analytik Jena) equipped with VisionWorks software. Images were processed using ImageJ (NIH).

489 **Cell Culture:** Human cardiac fibroblasts (hCFs) were obtained from Cell Applications (USA) at passage 1,
490 and cultured in Dulbecco's Modified Eagle Medium (DMEM) (Thermo Fisher) supplemented with 10% fetal
491 bovine serum (FBS) (Gibco), 1% penicillin/streptomycin (P/S) (Life Technologies), henceforth called DMEM
492 Complete, and 3 µM SD208, a TGF-β receptor I kinase inhibitor (Sigma Aldrich). Cells were cultured with
493 SD208 supplement to inhibit transdifferentiation, and then used between passage 4 and 10 without
494 SD208. Mouse cardiac fibroblasts (mCFs) were obtained from iX Cells Biotech (USA) at passage 0, and were
495 cultured under the same conditions as hCFs.

496 **Cell Uptake of EVs:** hCFs were seeded in a 24-well plate at 50,000 cells/well to allow for imaging of small
497 cell clusters without compromising cell viability. Three wells were seeded for each of two biological
498 replicates of LVVs (n = 6 wells) and an empty control. LVVs were stained with ExoGlow (System
499 Biosciences), according to the manufacturer's protocol. Briefly, LVV content was quantified with the

500 bicinchoninic acid (BCA) gold protein quantification assay (Thermo Fisher Scientific), and 25 µg of LVVs
501 was obtained from each sample and resuspended in 12 µL of provided reaction buffer. After, 2 µL of stain
502 was added and allowed to react for 30 min at RT. Stained LVVs or an empty control were then isolated in
503 a provided gradient column and resuspended in 2mL of DMEM with 1% P/S, according to the
504 manufacturer's protocol, for a final concentration of 12.5 µg/mL. During this, hCFs were incubated with
505 Cell Tracker Green (Thermo Fisher) in PBS for 30 min at 37°C. Stained cells were incubated in DMEM with
506 1% P/S with one group of LVVs or the control at 37°C for 24 h, and imaged at 3, 8, 16, and 24 h of
507 incubation. Before imaging, the conditioned media from each well was moved to a sterile container and
508 the cells were washed with PBS. Cells were imaged in PBS, and the removed media was replaced after
509 imaging.

510 **Gel Contraction Assay:** Collagen solution (1.5 mg/mL) was prepared by mixing rat tail collagen (9.33
511 mg/mL, Corning), 10x PBS, deionized (DI) water, and DMEM with 1% P/S at 2:1:8:3 ratio in a final volume
512 of 250 µL. Immediately before seeding, pH was adjusted to 7.4 with 1 M NaOH. All steps up to the addition
513 of cells were performed on ice to prevent premature gelation. Cells were washed with PBS, detached from
514 flasks using trypsin-EDTA (0.25%), and then resuspended at 1.5 million cells/mL in DMEM with 1% P/S.
515 Cell suspension was mixed thoroughly with the collagen solution at 1:1 ratio. The mixture was transferred
516 into a 24-well plate (300 µL/well) and incubated at 37 °C for 2 h to allow for gel formation. In addition to
517 five cell-encapsulated gels, one cell-free gel (loaded with FBS-free DMEM Complete without cells,
518 henceforth gel control) was included. Gels were then incubated in FBS-free DMEM Complete
519 supplemented with 12.5 µg/mL LVVs from one group, or a PBS blank containing no LVVs (control). The gel
520 control was fed with control media. Images were taken every 12 h for 48 h and the diameter of the gel
521 was measured along two sets of orthogonal axes. This experiment was repeated twice (3 repetitions total)
522 for each of the biological replicates (N = 2) for all cohorts.

523 **Wound Healing Assay:** Cells were seeded onto a 24-well plate at a density of 2×10^5 cells per well and
524 allowed to grow to >90% confluency. Once confluent, cells were washed with PBS and subjected to a
525 vertical wound by gently dragging a 1000 μ L pipette tip across the monolayer. Wells were assessed under
526 the microscope to ensure successful and consistent wounding. Typical wound width was approximately
527 600 μ m. The cells were then incubated in FBS-free DMEM Complete supplemented with 12.5 μ g/mL LVVs
528 or a PBS blank containing no LVVs (control). The wounds were then imaged immediately and every
529 subsequent 24 h for 96 h. Cells were incubated at 37 °C between imaging, and media was replaced after
530 48 h. Wound healing was assessed using ImageJ by percent reduction in wound width in three locations
531 over time. This experiment was performed twice (2 repetitions total) for both biological replicates (N = 2)
532 for all cohorts.

533 **Immunostaining:** At 96 h post-wounding, cells were washed with PBS and incubated in 4%
534 paraformaldehyde for 15 min, then in 0.1% Triton X-100 for 30 min, and then in 10% goat serum for 2 h,
535 all at RT and with PBS washes after each step. Cells were next incubated with rabbit anti-vimentin (Abcam)
536 and mouse anti- α -SMA (Abcam) primary antibodies (dilution: 1:100 in 5% goat serum) at 4 °C overnight.
537 The cells were then washed and incubated with Alexa Fluor 647-labelled anti-rabbit IgG and Alexa Fluor
538 488-labelled anti-mouse IgG secondary antibodies (dilution: 1:200 in 5% goat serum) at 4°C for 6 h. Finally,
539 the cells were incubated with DAPI (dilution: 1:1000 in PBS) for 15 minutes at RT and imaged with a
540 fluorescent microscope (Axio Observer.Z1, Zeiss).

541 **Profiling of Cytokines:** To remove any residual extraneous proteins, samples were purified using the CD9
542 Exo-Flow Capture Kit (System Biosciences) using the manufacturer-provided protocol. Briefly, the pellet
543 was resuspended in a solution of biotin-conjugated CD9 antibody and streptavidin-coupled magnetic
544 beads overnight at 4 °C. LVVs were isolated magnetically and washed, then eluted from the magnetic
545 beads. The LVV solution was worked up to 1% Triton X-100 and left at 4 °C overnight. The lysed LVV

546 solution was assessed using the Proteome Profiler Human XL Cytokine Array Kit (R&D Systems) as
547 described previously^{64,65}, for detection of 111 cytokines (Supplemental Figure S5, Supplemental Table S5).
548 Briefly, nitrocellulose membranes with the immobilized antibodies against 111 cytokines were blocked
549 according to manufacturer's instructions and incubated overnight at 4 °C with equal concentrations of
550 proteins, determined by BCA assay, from each sample. Membranes were then washed and incubated with
551 antibody cocktail solution for 1 h, with streptavidin-horseradish peroxidase (HRP) for 30 min, and with the
552 Chemiluminescence reagent mix for 1 min. Membranes were then imaged with a biomolecular imager
553 (ImageQuant LAS4000, GE Healthcare) using X-ray exposure for 5-10 min. Relative cytokine content was
554 determined by blot intensity analysis in ImageJ.

555 Gene Ontology Analysis (GOA) was performed on the obtained relative expression data. Comprehensive
556 analysis was performed using an online database via PANTHER Gene Ontology classification for biological
557 processes and enrichment analysis⁶⁶⁻⁶⁸. Data was extracted from the output dataset and graphed using R.
558 Proteomic interactions of the same relative expression data were also classified through KEGG-based
559 proteomapping software⁶⁹ and are presented as obtained.

560 **miRNA Isolation:** RNA was isolated from LVV's using the Total Exosome RNA & Protein Isolation Kit
561 (Thermo Fisher Scientific). Briefly, isolated LVV's were resuspended in exosome resuspension buffer and
562 incubated with an equal volume of denaturation solution at 4 °C for 5 min. The solution was then mixed
563 with an equal volume of Acid-Phenol:Chloroform by vortexing for 30 seconds and centrifuged for 5 min
564 at 15,000g. The resulting aqueous phase was extracted and combined with 1.25x volume of 100% ethanol,
565 then transferred to the provided spin column. The spin column was centrifuged at 10,000g for 15 seconds
566 to bind and wash the RNA, then the RNA was eluted in the provided elution solution and quantified via a
567 microvolume spectrophotometer (Nanodrop 2000, Thermo Fisher Scientific).

568 **miRNA PCR:** Isolated miRNA content was quantified by real time quantitative PCR (RT-qPCR) using the
569 miScript PCR Kit (Qiagen) with a CFX Connect Real-Time system (Bio-Rad). cDNA was prepared from 100
570 ng of RNA template, and the primers used were hsa-miR-125b-5p, hsa-miR-143-3p, hsa-miR-145-5p, hsa-
571 miR-199a-3p, hsa-miR-221-3p, and hsa-miR-222-3p (Supplemental Table S6). Results were quantified
572 relative to RNU6B, the recommended control. Non template controls were also used, and no signal was
573 detected from these controls.

574 **Profiling of Total miRNA Population:** Immediately following isolation, the eluted miRNA was
575 concentrated using 3 kDa microcentrifuge spin filters (Amicon). Briefly, the 100 μ L miRNA solution was
576 worked up to 420 μ L with RNase-free water and placed into a filter, then centrifuged at 14,000g for 90
577 minutes. Next, the filter was inverted into a fresh collection tube, and centrifuged at 8,000g for 2 minutes.
578 The resulting isolate is 20-25 μ L of concentrated miRNA, which was quantified by a microvolume
579 spectrophotometer. Concentrated miRNA was then prepared for miRNA profiling (NanoString) according
580 to the manufacturer's protocol. Briefly, the provided miRNA codeset was mixed with the provided
581 hybridization buffer to produce a master mix, and spike-in miRNA controls were prepared at 200 pm. In
582 order, the master mix, concentrated sample miRNA, spike-in miRNA, and provided probes were mixed in
583 a PCR plate and incubated at 65 °C for 16 h. The hybridized solution was then mixed with 15 μ L of provided
584 hybridization buffer, for a total volume of 30-35 μ L, and added to the provided microfluidic cartridge. The
585 assay was run with the provided protocol for total miRNA analysis, and data was processed and analyzed
586 using the provided software using the recommended settings.

587 **miRNA Transfection:** hCFs were seeded and wounded as above for the wound healing assay. After
588 wounding, cells were incubated with DMEM miRNA transfection media with either a cocktail of mimics of
589 identified miRNA of interest (miR-125, ACGGGUUAGGCUCUUGGGAGCU; miR-143,
590 UGAGAUGAAGCACUGUAGCUC; miR-199a, ACAGUAGUCUGCACAUUGGUUA; miR-222,

591 AGCUACAUCUGGCUACUGGGU; all miRvana) or a scramble miRNA control (Negative Control #2,
592 Ambion) at 40 nM. Transfection media was prepared with Lipofectamine 3000 according to the
593 manufacturer's specifications. Imaging and analysis were performed as above. After wounding, the
594 transfected cells were fixed, stained and imaged as above in immunostaining. Two independent
595 experiments with N = 3 biological replicates each were performed, with the later fixed at 48 h due to the
596 high rates of cell death observed beyond that time point.

597 **Hypoxia Assay:** hCFs were seeded as above for miRNA transfection assays and transfected with the
598 mentioned miRNAs for 24 hours to maximize miRNA uptake and minimize cell death. Randomly selected
599 plates were also incubated with BrdU (Abcam, 10 μ M) for proliferation assessment. Following this, hCFs
600 were transferred to deoxygenated glucose-free media (RPMI, Thermo Fisher) and subjected to hypoxia
601 for 3 hours, which we have previously shown is sufficient to induce MI-like cell death⁶⁵. BrdU-treated
602 plates were subsequently fixed and prepared for staining as described in immunostaining, and stained
603 with anti-BrdU (Abcam), while non-BrdU plates were stained with calcein AM and ethidium homodimer-
604 1 Live/Dead stains (Invitrogen, 1:1000) to quantify living and dead cells, respectively. Stained cells were
605 imaged as in immunostaining, and images were quantified in ImageJ.

606 **Statistical Analysis:** Results were analyzed by one-way analysis of variance (ANOVA) with post-hoc Tukey's
607 HSD, two-way ANOVA with post-hoc Tukey's multiple comparison test, or a two-tailed Student's t-test
608 with Welch's correction for unequal standard deviation. Values are presented as the mean \pm standard
609 deviation (SD) unless otherwise indicated, and differences were considered significant when $p \leq 0.05$.

610

611

612

613 **ACKNOWLEDGEMENTS**

614 The lyophilization of decellularized ECM was conducted at the Center for Environmental Science and
615 Technology (CEST) at the University of Notre Dame.

616 We thank the Biophysics Instrumentation (BIC) Core Facility for the use of Optima MAX-XP Tabletop
617 Ultracentrifuge.

618 The authors acknowledge the use of the Electron Microscopy Core of the Notre Dame Integrated Imaging
619 Facility, a designated core of the NIH-funded Indiana Clinical and Translational Sciences Institute.

620 The Nanoparticle Tracking Analysis was conducted using the NanoSight NS300 at the Harper Cancer
621 Research Institute (HCRI) Tissue Core Facility.

622 The schematics in some figures were created using BioRender.com

623 We thank Stanley Cheng, Zorlutuna Lab manager, for assisting in proofreading this manuscript prior to
624 submission

625 **AUTHOR CONTRIBUTIONS**

626 G.R., G.B., J.Y., and P.Z. designed research, G.R. performed research, G.R. analyzed data, G.B. and P.Z.
627 conducted review and editing, P.Z. provided funding, project administration, and resources, G.R. wrote
628 the paper.

629

630

631

632

633 REFERENCES

- 634 1. Rahimi, K., Duncan, M., Pitcher, A., Emdin, C. A. & Goldacre, M. J. Mortality from heart failure,
635 acute myocardial infarction and other ischaemic heart disease in England and Oxford: a trend
636 study of multiple-cause-coded death certification. *J Epidemiol Community Health* **69**, 1000–1005
637 (2015).
- 638 2. Law, M. R., Watt, H. C. & Wald, N. J. The underlying risk of death after myocardial infarction in
639 the absence of treatment. *Arch Intern Med* **162**, 2405–2410 (2002).
- 640 3. di Franco, S., Amarelli, C., Montalto, A., Loforte, A. & Musumeci, F. Biomaterials and heart
641 recovery: cardiac repair, regeneration and healing in the MCS era: a state of the ‘heart’. *J Thorac*
642 *Dis* **10**, S2346–S2362 (2018).
- 643 4. D’Anca, M. *et al.* Exosome Determinants of Physiological Aging and Age-Related
644 Neurodegenerative Diseases. *Front Aging Neurosci* **11**, 232 (2019).
- 645 5. Yusuf, S. *et al.* Effect of potentially modifiable risk factors associated with myocardial infarction in
646 52 countries (the INTERHEART study): case-control study. *Lancet* **364**, 937–952 (2004).
- 647 6. Anand, S. S. *et al.* Risk factors for myocardial infarction in women and men: insights from the
648 INTERHEART study. *Eur Heart J* **29**, 932–940 (2008).
- 649 7. Florio, M. C., Magenta, A., Beji, S., Lakatta, E. G. & Capogrossi, M. C. Aging, MicroRNAs, and Heart
650 Failure. *Curr Probl Cardiol* **45**, 100406 (2020).
- 651 8. Vaccarino, V. *et al.* Sex differences in mortality after acute myocardial infarction: changes from
652 1994 to 2006. *Arch Intern Med* **169**, 1767–1774 (2009).
- 653 9. Vaccarino, V., Krumholz, H. M., Yarzebski, J., Gore, J. M. & Goldberg, R. J. Sex differences in 2-
654 year mortality after hospital discharge for myocardial infarction. *Ann Intern Med* **134**, 173–181
655 (2001).
- 656 10. Kessler, E. L., Rivaud, M. R., Vos, M. A. & van Veen, T. A. B. Sex-specific influence on cardiac
657 structural remodeling and therapy in cardiovascular disease. *Biol Sex Differ* **10**, 7 (2019).
- 658 11. Piccinini, A. M. & Midwood, K. S. Illustrating the interplay between the extracellular matrix and
659 microRNAs. *Int J Exp Pathol* **95**, 158–180 (2014).
- 660 12. Basara, G., Ozcebe, S. G., Ellis, B. W. & Zorlutuna, P. Tunable Human Myocardium Derived
661 Decellularized Extracellular Matrix for 3D Bioprinting and Cardiac Tissue Engineering. *Gels* **7**,
662 (2021).
- 663 13. Fields, L. *et al.* Epicardial placement of human MSC-loaded fibrin sealant films for heart failure:
664 preclinical efficacy and mechanistic data. *Mol Ther* (2021) doi:10.1016/j.ymthe.2021.04.018.
- 665 14. Huang, K. *et al.* An off-the-shelf artificial cardiac patch improves cardiac repair after myocardial
666 infarction in rats and pigs. *Sci Transl Med* **12**, (2020).

- 667 15. Zhang, D. *et al.* Tissue-engineered cardiac patch for advanced functional maturation of human
668 ESC-derived cardiomyocytes. *Biomaterials* **34**, 5813–5820 (2013).
- 669 16. Zhu, D. *et al.* Minimally invasive delivery of therapeutic agents by hydrogel injection into the
670 pericardial cavity for cardiac repair. *Nat Commun* **12**, 1412 (2021).
- 671 17. Christman, K. L. *et al.* Injectable fibrin scaffold improves cell transplant survival, reduces infarct
672 expansion, and induces neovasculature formation in ischemic myocardium. *J Am Coll Cardiol* **44**,
673 654–660 (2004).
- 674 18. Traverse, J. H. *et al.* First-in-Man Study of a Cardiac Extracellular Matrix Hydrogel in Early and
675 Late Myocardial Infarction Patients. *JACC Basic Transl Sci* **4**, 659–669 (2019).
- 676 19. Johnson, T. D., Braden, R. L. & Christman, K. L. Injectable ECM scaffolds for cardiac repair.
677 *Methods Mol Biol* **1181**, 109–120 (2014).
- 678 20. Sicari, B. M. *et al.* The promotion of a constructive macrophage phenotype by solubilized
679 extracellular matrix. *Biomaterials* **35**, 8605–8612 (2014).
- 680 21. Yap, J., Cabrera-Fuentes, H. A., Irei, J., Hausenloy, D. J. & Boisvert, W. A. Role of Macrophages in
681 Cardioprotection. *Int J Mol Sci* **20**, (2019).
- 682 22. Zgheib, C., Xu, J. & Liechty, K. W. Targeting Inflammatory Cytokines and Extracellular Matrix
683 Composition to Promote Wound Regeneration. *Adv Wound Care (New Rochelle)* **3**, 344–355
684 (2014).
- 685 23. Xu, M. Y., Ye, Z. S., Song, X. T. & Huang, R. C. Differences in the cargos and functions of exosomes
686 derived from six cardiac cell types: a systematic review. *Stem Cell Res Ther* **10**, 194 (2019).
- 687 24. Dubnika, A. *et al.* Cytokines as therapeutic agents and targets in heart disease. *Cytokine Growth*
688 *Factor Rev* **43**, 54–68 (2018).
- 689 25. Mehra, V. C., Ramgolam, V. S. & Bender, J. R. Cytokines and cardiovascular disease. *J Leukoc Biol*
690 **78**, 805–818 (2005).
- 691 26. Huleihel, L. *et al.* Matrix-bound nanovesicles within ECM bioscaffolds. *Sci Adv* **2**, (2016).
- 692 27. Yáñez-Mó, M. *et al.* Biological properties of extracellular vesicles and their physiological
693 functions. *J Extracell Vesicles* **4**, 27066 (2015).
- 694 28. An, M. *et al.* Extracellular matrix-derived extracellular vesicles promote cardiomyocyte growth
695 and electrical activity in engineered cardiac atria. *Biomaterials* **146**, 49–59 (2017).
- 696 29. Huleihel, L. *et al.* Matrix-Bound Nanovesicles Recapitulate Extracellular Matrix Effects on
697 Macrophage Phenotype. *Tissue Eng Part A* **23**, 1283–1294 (2017).
- 698 30. Eitan, E. *et al.* Age-Related Changes in Plasma Extracellular Vesicle Characteristics and
699 Internalization by Leukocytes. *Sci Rep* **7**, 1342 (2017).

- 700 31. Joris, V. *et al.* MicroRNA-199a-3p and MicroRNA-199a-5p Take Part to a Redundant Network of
701 Regulation of the NOS (NO Synthase)/NO Pathway in the Endothelium. *Arterioscler Thromb Vasc*
702 *Biol* **38**, 2345–2357 (2018).
- 703 32. Lee, D. S. *et al.* Defined MicroRNAs Induce Aspects of Maturation in Mouse and Human
704 Embryonic-Stem-Cell-Derived Cardiomyocytes. *Cell Rep* **12**, 1960–1967 (2015).
- 705 33. Ottaviani, L., Sansonetti, M. & da Costa Martins, P. A. Myocardial cell-to-cell communication via
706 microRNAs. *Noncoding RNA Res* **3**, 144–153 (2018).
- 707 34. Prathipati, P., Nandi, S. S. & Mishra, P. K. Stem Cell-Derived Exosomes, Autophagy, Extracellular
708 Matrix Turnover, and miRNAs in Cardiac Regeneration during Stem Cell Therapy. *Stem Cell Rev*
709 *Rep* **13**, 79–91 (2017).
- 710 35. Perel, P. *et al.* Comparison of treatment effects between animal experiments and clinical trials:
711 systematic review. *BMJ* **334**, 197 (2007).
- 712 36. Yang, J., Bahcecioglu, G. & Zorlutuna, P. The Extracellular Matrix and Vesicles Modulate the
713 Breast Tumor Microenvironment. *Bioengineering (Basel)* **7**, (2020).
- 714 37. Caponnetto, F. *et al.* Size-dependent cellular uptake of exosomes. *Nanomedicine* **13**, 1011–1020
715 (2017).
- 716 38. Wang, M., Baker, L., Tsai, B. M., Meldrum, K. K. & Meldrum, D. R. Sex differences in the
717 myocardial inflammatory response to ischemia-reperfusion injury. *Am J Physiol Endocrinol Metab*
718 **288**, E321-6 (2005).
- 719 39. Rea, I. M. *et al.* Age and Age-Related Diseases: Role of Inflammation Triggers and Cytokines. *Front*
720 *Immunol* **9**, (2018).
- 721 40. Baum, J. & Duffy, H. S. Fibroblasts and myofibroblasts: what are we talking about? *J Cardiovasc*
722 *Pharmacol* **57**, 376–379 (2011).
- 723 41. Bujak, M. & Frangogiannis, N. G. The role of IL-1 in the pathogenesis of heart disease. *Arch*
724 *Immunol Ther Exp (Warsz)* **57**, 165–176 (2009).
- 725 42. Wang, M. & Shah, A. M. Age-associated pro-inflammatory remodeling and functional phenotype
726 in the heart and large arteries. *J Mol Cell Cardiol* **83**, 101–111 (2015).
- 727 43. Ndrepepa, G. Myeloperoxidase - A bridge linking inflammation and oxidative stress with
728 cardiovascular disease. *Clin Chim Acta* **493**, 36–51 (2019).
- 729 44. Ma, F. *et al.* Macrophage-stimulated cardiac fibroblast production of IL-6 is essential for TGF
730 β /Smad activation and cardiac fibrosis induced by angiotensin II. *PLoS One* **7**, e35144 (2012).
- 731 45. Schafer, S. *et al.* IL-11 is a crucial determinant of cardiovascular fibrosis. *Nature* **552**, 110–115
732 (2017).
- 733 46. Yabluchanskiy, A., Ma, Y., Iyer, R. P., Hall, M. E. & Lindsey, M. L. Matrix metalloproteinase-9:
734 Many shades of function in cardiovascular disease. *Physiology (Bethesda)* **28**, 391–403 (2013).

- 735 47. Bernhagen, J. Protective cardiac conditioning by an atypical cytokine. *Clin Sci (Lond)* **133**, 933–937
736 (2019).
- 737 48. Dewitte, K. *et al.* Role of oxidative stress, angiogenesis and chemo-attractant cytokines in the
738 pathogenesis of ischaemic protection induced by remote ischaemic conditioning: Study of a
739 human model of ischaemia-reperfusion induced vascular injury. *Pathophysiology* **26**, 53–59
740 (2019).
- 741 49. Fan, Z. & Guan, J. Antifibrotic therapies to control cardiac fibrosis. *Biomater Res* **20**, 13 (2016).
- 742 50. Jahangir, A., Sagar, S. & Terzic, A. Aging and cardioprotection. *J Appl Physiol (1985)* **103**, 2120–
743 2128 (2007).
- 744 51. Shimizu, M. *et al.* Remote ischemic preconditioning decreases adhesion and selectively modifies
745 functional responses of human neutrophils. *J Surg Res* **158**, 155–161 (2010).
- 746 52. Varga, Z. v, Ágg, B. & Ferdinandy, P. miR-125b is a protectomiR: A rising star for acute
747 cardioprotection. *J Mol Cell Cardiol* **115**, 51–53 (2018).
- 748 53. Ma, W. Y. *et al.* Melatonin promotes cardiomyocyte proliferation and heart repair in mice with
749 myocardial infarction via miR-143-3p/Yap/Ctnd1 signaling pathway. *Acta Pharmacol Sin* **42**,
750 921–931 (2021).
- 751 54. Zhao, W., Zhao, S. P. & Zhao, Y. H. MicroRNA-143/-145 in Cardiovascular Diseases. *Biomed Res Int*
752 **2015**, 531740 (2015).
- 753 55. Li, B. & Wang, J. H. Fibroblasts and myofibroblasts in wound healing: force generation and
754 measurement. *J Tissue Viability* **20**, 108–120 (2011).
- 755 56. Vaughan, M. B., Odejimi, T. D., Morris, T. L., Sawalha, D. & Spencer, C. L. A new bioassay
756 identifies proliferation ratios of fibroblasts and myofibroblasts. *Cell Biol Int* **38**, 981–986 (2014).
- 757 57. Liu, B. *et al.* Cardiac recovery via extended cell-free delivery of extracellular vesicles secreted by
758 cardiomyocytes derived from induced pluripotent stem cells. *Nat Biomed Eng* **2**, 293–303 (2018).
- 759 58. Kishore, A., Borucka, J., Petrková, J. & Petrek, M. Novel insights into miRNA in lung and heart
760 inflammatory diseases. *Mediators Inflamm* **2014**, 259131 (2014).
- 761 59. Noetel, A., Kwiecinski, M., Elfimova, N., Huang, J. & Odenthal, M. microRNA are Central Players in
762 Anti- and Profibrotic Gene Regulation during Liver Fibrosis. *Front Physiol* **3**, 49 (2012).
- 763 60. Lee, B. R., Kim, J. H., Choi, E. S., Cho, J. H. & Kim, E. Effect of young exosomes injected in aged
764 mice. *Int J Nanomedicine* **13**, 5335–5345 (2018).
- 765 61. Wang, W. *et al.* Extracellular vesicles extracted from young donor serum attenuate inflammaging
766 via partially rejuvenating aged T-cell immunotolerance. *FASEB J* fj201800059R (2018)
767 doi:10.1096/fj.201800059R.

- 768 62. Théry, C. *et al.* Minimal information for studies of extracellular vesicles 2018 (MISEV2018): a
769 position statement of the International Society for Extracellular Vesicles and update of the
770 MISEV2014 guidelines. *J Extracell Vesicles* **7**, 1535750 (2018).
- 771 63. Webber, J. & Clayton, A. How pure are your vesicles? *J Extracell Vesicles* **2**, (2013).
- 772 64. Bahcecioglu, G. *et al.* Aged Breast Extracellular Matrix Drives Mammary Epithelial Cells to an
773 Invasive and Cancer-Like Phenotype. *bioRxiv* 2020.09.30.320960 (2020)
774 doi:10.1101/2020.09.30.320960.
- 775 65. Ozcebe, S. G., Bahcecioglu, G., Yue, X. S. & Zorlutuna, P. Effect of cellular and ECM aging on
776 human iPSC-derived cardiomyocyte performance, maturity and senescence. *Biomaterials* **268**,
777 120554 (2021).
- 778 66. Ashburner, M. *et al.* Gene ontology: tool for the unification of biology. The Gene Ontology
779 Consortium. *Nat Genet* **25**, 25–29 (2000).
- 780 67. Consortium, G. O. The Gene Ontology resource: enriching a GOld mine. *Nucleic Acids Res* **49**,
781 D325–D334 (2021).
- 782 68. Mi, H., Muruganujan, A., Ebert, D., Huang, X. & Thomas, P. D. PANTHER version 14: more
783 genomes, a new PANTHER GO-slim and improvements in enrichment analysis tools. *Nucleic Acids*
784 *Res* **47**, D419–D426 (2019).
- 785 69. Liebermeister, W. *et al.* Visual account of protein investment in cellular functions. *Proc Natl Acad*
786 *Sci U S A* **111**, 8488–8493 (2014).
- 787